Effect of particles with repulsive interactions enclosed in both rigid spherical shells and flexible fluid vesicles studied by Monte Carlo simulation

Hibiki Itoga,[1,*] Ryota Morikawa,[1,†] Tsuyoshi Ueta,[2] Takeshi Miyakawa,[1] Yuno Natsume,[3] and Masako Takasu[1]
[1]*Tokyo University of Pharmacy and Life Sciences, Tokyo 192-0392, Japan*
[2]*Jikei University, Tokyo 182-0022, Japan*
[3]*Japan Women's University, Tokyo 112-8681, Japan*

(Received 11 June 2018; revised manuscript received 7 February 2019; published 25 April 2019)

Experimental observations indicate that the repulsion of particles is a factor that induces the transformation of vesicles containing multiple particles. Metropolis Monte Carlo simulations are performed with two models in which repulsive particles are enclosed inside a vesicle. The distribution of the particles and the effective bending coefficient and surface tension of the membrane are analyzed. The shape and internal structure of the vesicle containing the particles are investigated as the vesicle volume is decreased. It is revealed that the repulsive interaction between particles produces a layered structure and stiffens the membrane. When particles repulsively interact over a long range, the membrane takes on a dumbbell form.

DOI: 10.1103/PhysRevE.99.042418

I. INTRODUCTION

Flexible membranes and soft particles are important in molecular biology. The cell is a structure separated from an environment by a flexible lipid bilayer membrane, which contains several kinds of cytosolic molecules at a high density [1]. These molecules inside the membrane exhibit specific or nonspecific interaction with other molecules and increase the viscosity within the cell [1]. Most organelles inside the cell have membrane structures. The relationship between the membrane deformation and behavior of internal molecules has attracted attention. The physical understanding of this relationship is crucial for investigating biological phenomena, such as division and secretion. Computational studies aimed toward the complete understanding of this dynamic behavior will require a detailed understanding of the structure and properties of each molecule contained in the membrane. For this reason, simple cell models were prepared *in vitro*, which are giant bilayer vesicles containing polystyrene latex beads [2,3] (PSLBs), polyethylene glycol (PEG), or dextran [4]. It was observed that giant vesicles containing a high concentration of PSLBs transform into a shape resembling a pearl necklace or polyhedrons when the excess area and the volume fraction of the particles increase due to increased external osmotic pressure [2,3]. The average diameters of the vesicle and the included particles are about 10 and 1 μm, respectively, and the included particles are negatively charged.

In addition, it has been observed that giant vesicles including a high concentration of PEG or dextran transform into a pearl-necklace-like shape when the excess area increases through the fusion of vesicles caused by an electric pulse [4]. These transformation phenomena are induced by the included particles. In the reported experiments [2–4], particle-particle or membrane-particle adsorption was not investigated. Although the studied systems contained particles (PSLBs, PEG, or dextran) of varying surface and size properties, transformations were observed in each of the three systems. Because the shape of the vesicle changes to increase the free volume of the included particles [2–4], the depletion interaction [5–9] was used to explain the transformation [4]. When a suspension contains large and small colloidal particles, an effective attractive force between the large particles occurs. This is an entropic force called the depletion force. The origin of the depletion interaction is the repulsion between particles. If particles are deformable, the amount of interaction strongly increases [10]. The interaction is observed not only in the famous case of a suspension containing large and small particles, but also in the case of the vesicle and included particles [8]. In this case, to maximize the free volume of the particles, the curvature of the membrane is frequently varied. When the membrane is curved, the excluded volume is reduced. Therefore, the situation is more complicated than in a hard-sphere system. The free energy of the depletion interaction decreases proportionally to the osmotic pressure of the colloidal particles and the logarithm of the free volume of the included particles. Considering both the depletion interaction and the curvature elastic energy of the membrane, Terasawa and others showed that the free energy of the twin-shaped vesicles is lower than that of spherocylinders when the surface area and volume of the two shapes are the same [4]. The free energy for other shapes was not obtained. However, the state obtained by minimizing the steric repulsive potential between colloidal particles will be determined to increase the free volume of colloidal particles. Therefore, it is not clear whether this increase in free volume is induced by depletion interaction.

To analyze the shape of a giant vesicle, the continuous membrane models are useful [11]. In these models, the following four conditions are assumed: First, the change in the area of the lipid membrane is small in the equilibrium state.

*s096020@toyaku.ac.jp
†morikawa@toyaku.ac.jp

Second, the lipid bilayer does not split. Third, lipid exchange between two lipid layers is very slow [12]. Fourth, the lipid membrane thickness is sufficiently small compared with the size of the membrane. In order to introduce the curvature elasticity that a membrane exhibits naturally, two types of elastic models have been considered. The spontaneous curvature model was constructed by Canham *et al.* [13,14]; this model includes the curvature-dependent bending energy. This energy is generated by the effect of the repulsive or attractive forces between neighboring lipid molecules [15]. The most stable shape of the vesicle as a function of the spontaneous curvature was systematically investigated [16]. The area-difference elasticity (ADE) model is a variation of the spontaneous curvature model using the ADE energy [17]. The ADE energy is related to the mismatch of the area differences of the bilayer of the vesicle and of its spontaneous shape [17,18]. The most stable shape of the vesicle as a function of the optimal area difference was also systematically investigated [17,19]. The shape transitions observed in experiments [19,20] can be explained using the ADE model [20,21].

Both models are often applied to axisymmetric models and triangulated lattice models [22]. Nonaxisymmetric models are more appropriate than axisymmetric ones for investigating the shape of a model corresponding to an actual vesicle [19,21,23]. A triangular lattice with tethering exchange is called the fluid membrane. The fluid membrane has been studied carefully for a long time. The structure and scaling behavior of the self-avoiding fluid membrane at equilibrium with bending rigidity module κ were investigated using Monte Carlo simulation [24,25], indicating that the membrane softens according to the size. The effective restriction on the shape of the fluid vesicle is small. For this reason, a study of driven transport of fluid membranes through narrow pores was performed [26]. A budding structure is obtained in the fluid vesicles, which is extended to a model of multicomponent vesicles [27]. When calculating the bending elastic energy of this polyhedron membrane by using the inner products of surface normals of neighboring faces, an error occurs in cases such as the spherocylinder [28]. Gompper and Kroll have solved this problem by using Itzykson-type discretization [28,29].

For a quasispherical vesicle, the excess bending energy was estimated from the membrane fluctuation using the spherical harmonic expansion with a constant-surface-area assumption [30]. However, when applying the technique including this approximation to the actual vesicles or the fluid vesicles, the estimated excess bending energy includes the surface tension energy corresponding to a small area change. It has become possible to describe the membrane fluctuating in a certain area by employing a Lagrange multiplier as the effective surface tension [31]. Based on this method, the excess energy was split into the excess bending energy and the excess surface tension. For the vesicle including repulsive particles, estimation of both the Lagrange multiplier of the effective bending coefficient and the effective surface tension is not easy from the virial corresponding to the gradient of a repulsive energy between particles.

Studies were conducted considering the pressure difference between the inside and the outside of a vesicle [32], as well as the pressure difference between the inside and the outside of a vesicle containing colloidal particles [33,34]. Neither study explicitly encapsulated the particles. When the osmotic pressure difference is zero and the temperature is finite, the frequency of prolates or oblates is high and the frequency of the sphere that has the lowest energy is low [33]. On the other hand, when the external pressure was high, it was shown that the most frequent shape coincides with the energetically expected shape [33]. When the inner pressure was increased, the surface tension increased continuously from a fluctuating state to a limited shape with the maximum volume [34]. In this transition, the surface tension becomes appreciable.

The Markov chain Monte Carlo method based on the Metropolis algorithm is often used for simulation of a vesicle at equilibrium. In this method, the states around the local minima are searched using the Markov chain. The range of the states depends on the system temperature. In this method, it is not necessary to derive a force; thus, it can be easily applied to simulation. It cannot be used to investigate dynamics, but it is useful for obtaining the equilibrium state. In the simulation of a vesicle using the Metropolis algorithm, a new state is created by moving the grid points of the fluid membrane and dynamic tethering exchange. Removing an arbitrary state from the chain is useful for improving the search efficiency and for keeping the mesh in a preferable state. In order to realize this, infinite potential was introduced [22,28,35,36]. If a wide range of tethering lengths is allowed, the number of tethers corresponding to the grid points tends to be irregular. As a result, the effective bending rigidity becomes locally different [37]. Therefore, the tethering length is restricted to the extent of the range by using infinite potential. Even if a restraint of the tethering length is imposed, it is possible to make a branch with a diameter of approximately the tethering length.

Theoretically, it is proven that the effective pair potential between charged colloids is repulsive [38]. Therefore, the charged colloids and the hard spheres have some similarity. It is reported that in a study using the Monte Carlo method and thermodynamic integration, the interfacial free energy of particles near the hard plate becomes higher nonlinearly as a function of the volume fraction of the hard spheres [39]. A similar free energy should be seen in the system of the vesicle and repulsive particles. The phase behavior of hard spheres sandwiched between parallel hard walls [40] and the ordered structure of hard spheres surrounded by a wedge-shaped hard shell [41] were examined. In the experiment, ordered particles near the membrane can be seen in the system of the vesicle and PSLBs [3].

Models of a triangulated vesicle including spherical particles were constructed in previous studies [42,43], which were focused on the attractive interaction between the particles and the membrane. In addition, the effect of the attractive interaction was found to be significant, causing the local membrane to deform to fit the particles [42,43].

In our previous study [44], we investigated a system enclosing rigid spheres inside an Itykson-type discretized vesicle via the ADE model and analyzed the vesicle shape for various values of the number of particles and the optimal area difference. In that simulation, no remarkable change in shape was observed. The effect that the rigid spheres have on the shape of the vesicle is expected to be smaller than the effect

of deformable particles [10]. In fact, particles which induced the remarkable deformation, PSLBs, PEG, and dextran, are charged colloid particles or deformable particles [2], and PEG is a flexible molecule [4]. Because the repulsive effect of the hard particles is less than that of actual particles with electrostatic repulsion, we considered that the deformation of the vesicle including hard spheres [44] is smaller than the actual deformation.

In order to analyze the dynamic deformation of the vesicle, simulation studies using molecular dynamics have been performed. For example, the shape change of the vesicle in the capillary was investigated [45]. In addition, a simulation to analyze the structure of cells containing molecules was performed using the dissipative particle dynamics technique [46]. However, in these simulations, it is difficult to reproduce the deformation of vesicles on a time scale of seconds to minutes as observed in experiments [2,3,4].

On the other hand, in order to analyze the shapes of the vesicles at equilibrium and fluctuations under given conditions, the Metropolis Monte Carlo (MMC) method has been employed [22,24,28,32,33,35,36,43,47,48]. The MMC method is simpler and provides faster calculation for equilibrium sampling than the molecular dynamics method because the gradient information of a potential field is unnecessary. Therefore, in simulations, it is possible to avoid the error in calculating forces depending on the curvature [49].

The objective of this paper is to study the shape of a fluid vesicle containing repulsive particles. In order to investigate the interaction between particles and membrane, we take three approaches to the problem. First, we analyze the distribution of particles because it is expected that the ordering of particles will appear inside the vesicle as in the study by Tata *et al.* [41]. Second, we estimated the effective bending coefficient and the effective surface tension from the fluctuation of the vesicular membrane in order to investigate the dependency on the number of particles and on the exponent of repulsion on the membrane. Finally, the phase diagram is created to investigate the shape of the fluid vesicle including particles depending on the number of particles and the exponent of repulsion when the volume of the vesicle decreases.

II. MODELS OF VESICLES CONTAINING PARTICLES

Two models of the vesicle including particles were constructed, as shown in Fig. 1. The membrane of each vesicle model has infinite or finite bending coefficients κ. The unit length of the system is σ, and the unit of energy of the system is k_BT so that each prefactor of energy f_R, κ, $\bar{\kappa}$, f_A, and $\Delta\mu$, which appears later, is scaled by k_BT.

A. Rigid spherical shell and particles model

The rigid spherical shell and particles (RSSP) model has a rigid spherical shell as the membrane with the bending rigidity coefficient $\kappa \to \infty$. If the area of the membrane is constant, the shape of the vesicle is spherical. N_p particles with diameters σ_p are encapsulated inside this rigid shell. This model possesses a wall potential energy E_W and repulsive energy E_R between the particles. Thus, the total energy is

$$E_{RSSP} = E_W + E_R. \tag{1}$$

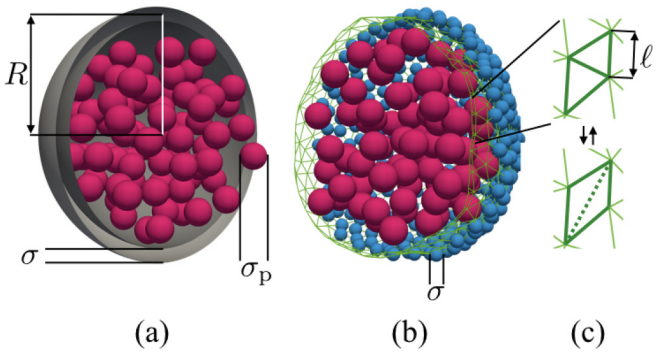

FIG. 1. Two models of a vesicle that contains particles. (a) RSSP model. R and σ are the radius and thickness of the shell, respectively. σ_p is the diameter of the included particle. (b) TLP model. The exclusive volume of a vertex of the triangulated lattice is a sphere of diameter σ. (c) The tethers of the lattice network are dynamically changed. ℓ is the tethering length.

The center of the shell is $\boldsymbol{O}$, and its radius and thickness are R and σ, respectively. The wall potential energy for the position $\boldsymbol{P}_i$ of the ith particle is

$$V_W(\boldsymbol{P}_i) = \begin{cases} 0 & \text{for} \quad ||\boldsymbol{P}_i - \boldsymbol{O}|| < R - \dfrac{\sigma + \sigma_p}{2}, \\ \infty & \text{otherwise.} \end{cases} \tag{2}$$

The sum of the wall potential energy of each particle is $E_W = \sum_{i=1}^{N_p} V_W(\boldsymbol{P}_i)$.

The repulsive potential energy between the ith and the jth particles is given by

$$V_R(d_{ij}) = f_R \left(\frac{\sigma_p}{d_{ij}}\right)^n, \tag{3}$$

where f_R is the strength and d_{ij} is the distance between the ith and the jth particles. The exponent n is regarded as the softness of the particles. Considering the case in which particles exist in three-dimensional infinite space at a constant density, the potential energy of a particle diverges in the case of $n < 3$. Therefore, the case of $n < 3$ is long-range repulsion, and the case of $n \geqslant 3$ is short-range repulsion. The total repulsive energy is $E_R = \sum_{i \neq j}^{N_p} V_R(d_{ij})$.

B. Triangular lattice and particles model

For modeling the flexible vesicle and particles, we used a closed triangular lattice and soft particles and called it the triangular lattice and particles (TLP) model. The total energy of the model is

$$E_{TLP} = E_{SA} + E_T + E_B + E_{ADE} + E_A + E_V + E_R. \tag{4}$$

In order to consider the self-avoidance of the membrane, the self-avoiding energy of the vertices and restriction of the tethering length between the pairs of vertices are required. Each vertex of the vesicle has an exclusive volume with a diameter σ. The tethering length ℓ_{ij} of the ith and jth particles within the vesicle is restricted to $1 \leqslant \ell_{ij} < \sqrt{3}$.

The total self-avoiding energy of the vesicle and particles is written as

$$E_{\mathrm{SA}} = \sum_{i=1}^{N}\sum_{\substack{j=1\\ j\neq i}}^{N} V_{\mathrm{SA}}^{\mathrm{vv}}(L_{ij}) + \sum_{i=1}^{N}\sum_{k=1}^{N_{\mathrm{p}}} V_{\mathrm{SA}}^{\mathrm{vp}}(s_{ik}), \tag{5}$$

$$V_{\mathrm{SA}}^{\mathrm{vv}}(L_{ij}) = \begin{cases} \infty & \text{if} \quad L_{ij} \leqslant \sigma, \\ 0 & \text{otherwise}, \end{cases} \tag{6}$$

$$V_{\mathrm{SA}}^{\mathrm{vp}}(s_{ik}) = \begin{cases} \infty & \text{if} \quad s_{ik} \leqslant (\sigma + \sigma_{\mathrm{p}})/2, \\ 0 & \text{otherwise}, \end{cases} \tag{7}$$

where N is the number of vertices, L_{ij} is the distance between the ith and the jth vertices, and s_{ik} is the distance between the ith vertex and the kth particle.

The potential energy for the restriction of the tethering length is [22]

$$E_{\mathrm{T}} = \frac{1}{2}\sum_{i=1}^{N}\sum_{j(i)} V_{\mathrm{T}}(\ell_{ij}), \tag{8}$$

with

$$V_{\mathrm{T}}(\ell_{ij}) = \begin{cases} 0, & \ell_{ij} < \ell_{\max} \quad \text{for a connected neighboring} \\ & \text{vertex pair}, \\ \infty & \text{otherwise}. \end{cases} \tag{9}$$

Here, $j(i)$ is the index of the connected neighboring vertices of the ith vertex and $\ell_{\max}$ is the maximum tethering length. To avoid penetration of the membrane, $\ell_{\max} \leqslant \sqrt{3}$ is required.

The bending elastic energy E_{b} of the lipid bilayer membrane, disregarding the energy of the higher-order terms, is [13,14,50]

$$E_{\mathrm{b}} = \int_A \mathrm{d}A\left[\frac{\kappa}{2}(H - C_0)^2 + \kappa_{\mathrm{G}}K\right], \tag{10}$$

where H in the first term of the surface integral is the mean curvature. The spontaneous curvature C_0 is 0 when the lipid numbers of the inner and outer layers are equal. In the second term, κ_{G} and K are the Gaussian bending coefficient and Gaussian curvature, respectively. In our model, the topology of the vesicle does not change. In this case, the integral value of the second term is constant. We consider the case of a vesicle with a fixed topology and $C_0 = 0$. Then, from Eq. (10), the discrete bending curvature energy of the vesicle becomes [28,29]

$$E_{\mathrm{B}} = \frac{\kappa}{2}\sum_{i=1}^{N} H_i^2 b_i. \tag{11}$$

The mean curvature H_i and the small area b_i for the ith vertex are written as

$$H_i = \frac{1}{b_i}\boldsymbol{n}_i \cdot \sum_{j(i)} \frac{m_{ij}}{l_{ij}}(\boldsymbol{x}_i - \boldsymbol{x}_j) \tag{12}$$

and

$$b_i = \frac{1}{4}\sum_{j(i)} m_{ij} l_{ij}. \tag{13}$$

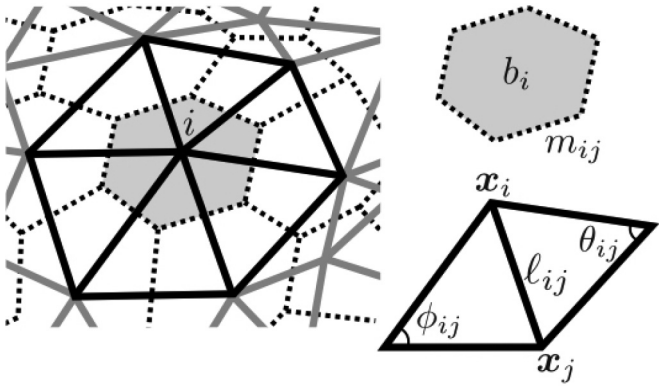

FIG. 2. Illustration of the fluid membrane around the ith vertex. The triangulated lattice of the vesicle is shown by solid lines. The virtual dual lattice in Ref. [29] is shown by dotted gray lines. The length of the edge perpendicular to the link (i, j) is m_{ij}. The area of the dual lattice cell for the ith vertex is b_i.

To obtain a vertex normal of the ith vertex $\boldsymbol{n}_i$, we added the surface normal vectors of the triangles that contain the ith vertex, and the result was normalized to acquire a vector of unit length. $m_{ij} = \ell_{ij}[\cot(\theta_{ij}) + \cot(\phi_{ij})]/2$, where θ_{ij} and ϕ_{ij} are the angles of the opposite tether of the ith and jth vertices, respectively, and $\boldsymbol{x}_i$ is the position of the ith vertex, as shown in Fig. 2.

The ADE energy is determined by the area difference between the outer and the inner lipid layers ΔA and the optimal area difference ΔA_0, which depends on the number of molecules in each layer, and is given as

$$E_{\mathrm{ADE}} = \frac{\bar{\kappa}}{2}\frac{\pi}{A\zeta^2}(\Delta A - \Delta A_0)^2, \tag{14}$$

where $\bar{\kappa}$ is the bending coefficient and ζ is the thickness of the bilayer [17]. The area difference is written by the mean curvature as

$$\Delta A = \zeta \int_A H \mathrm{d}A. \tag{15}$$

The equation ignores lipid exchange between lipid layers (flip-flop) because it is assumed that the exchange of lipid molecules is sufficiently slow compared with the time scale of the membrane transformations. When the dimensionless area difference $\Delta a = \int H \mathrm{d}A/(8\pi\sqrt{A/4\pi})$ is introduced, we obtain

$$E_{\mathrm{ADE}} = 8\pi^2\bar{\kappa}(\Delta a - \Delta a_0)^2. \tag{16}$$

To restrict the surface area A of the membrane, we introduce a constraint energy as

$$E_A = f_{\mathrm{A}}(A - A_0)^2, \tag{17}$$

where f_{A} is the constraint coefficient and A_0 is the optimal area, for which every tethering length is equal to $(\sigma + \ell_{\max})/2$.

To restrict the volume of the vesicle, we introduce the volume energy E_V, written as

$$E_V = \Delta\mu\left\{V - \frac{4\pi}{3}\left(\frac{\sigma_{\mathrm{p}}}{2}\right)^3 N_{\mathrm{p}}\right\}. \tag{18}$$

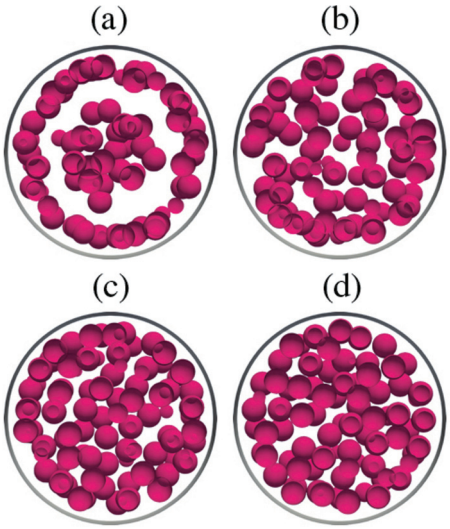

FIG. 3. Sliced snapshots of the equilibrium state of the system of the rigid spherical shell system with $N_p = 200$ particles and $\Delta\mu = 0$. The exponents n of repulsion are (a) 1, (b) 3, (c) 6, and (d) 12.

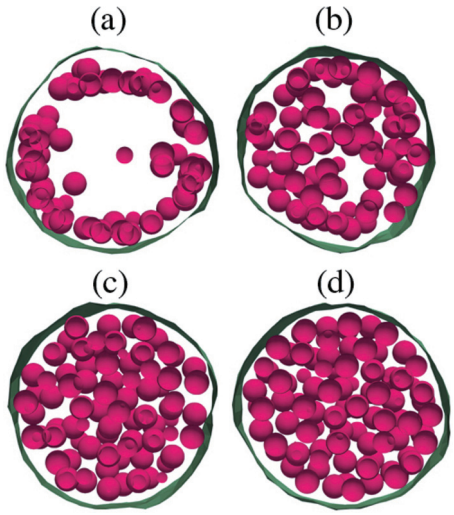

FIG. 4. Sliced snapshots of the equilibrium state of the triangle lattice system with $N_p = 200$ particles and $\Delta\mu = 0$. The exponents n of repulsion of (a) 1, (b) 3, (c) 6, and (d) 12.

Here, $\Delta\mu = \mu_{out} - \mu_{in}$ is the osmotic pressure difference between the outside and the inside of the vesicle, and V is its volume.

To reduce the mechanical rigidity [37], dynamic tethering exchange [47] is applied to random pairs of triangles that share an edge.

III. SIMULATIONS

To evaluate the distribution of the particles, simulations based on the RSSP and TLP models were performed. To investigate the stiffness of the membrane, only the TLP model was used.

The simulations with both the RSSP and the TLP models were performed based on the MMC method. Random displacements of the particles and vertices of the vesicle were adopted with a probability $\min[1, \exp(-\Delta E)]$, which depends on the change in energy ΔE for each trial. Here, $\exp(-\Delta E)$ is the Boltzmann factor. The maximum displacement Δd_v was set to 0.1 for each vertex. In addition, to incorporate the effect of the viscous fluid [51], the maximum displacement Δd_p of each particle was defined as $\sqrt{\sigma/\sigma_p}\Delta d_v$. In the choice of the maximum displacement for particle corresponding to that for vertex, we employed the Stokes-Einstein equation. This rough approximation of assuming a sphere for particles and vertices is required since the diffusion coefficients are not obtained experimentally. We defined 1 Monte Carlo step (MCS) as a step unit during which every vertex and particle are moved, on average, once. Random tethering exchange was performed $N_t = N/10$ times for each MCS. This number was determined empirically, with various N_t values for sufficient relaxation of the lattice. Here, pseudorandom numbers were generated using the Mersenne Twister method [52]. We set $\sigma_p = 2$ by the ratio between the diameters of the giant vesicle and the PSLB [2].

For the RSSP model, we set the radius and the thickness of the shell as 8.5 and 1, respectively. These parameters correspond to the radius of the vesicle and the diameter of the particles in the TLP model. The number of particles N_p ranged from 1 to 210. For hard-sphere particles, the volume fraction of $N_p = 210$ particles is about 0.4. The exponent of the repulsion was selected as $n = 1$, 3, 6, and 12. The case of $n = 1$ corresponds to long-range repulsion, whereas $n = 3$, 6, and 12 correspond to short-range repulsion. The case of $n = 3$ is a crossover between the two ranges. The strength coefficient of the repulsion f_R was set to 1. If the distance of a particle pair was smaller than σ_p, then the energy was greater than 1. Five simulation runs were carried out with various random numbers for every condition. The initial structure was prepared using the closest packed particles inside the shell and subsequently randomly erasing excess particles.

The initial structure for the simulation based on the TLP model was constructed by filling N_p particles inside a spherical vesicle. In the simulation, the vesicle had $N = 642$ vertices, $\ell_{max} = \sqrt{2.5}$, $\kappa = 10$, $\bar{\kappa} = 10$, $\Delta a_0 = 1$, $f_A = 10$, and $\Delta\mu = 0$. Under these conditions with $N_p = 0$, it was clear that the optimal shape of the vesicle is a sphere with a radius of 8.5. If we set σ to the actual membrane thickness, the calculation time will be too long. Moreover, the effective exclusive area of the membrane to internal particles is not clear.

In addition, by means of changing the osmotic pressure $\Delta\mu$, shape transformations were investigated. During the simulation, the volume of the vesicle was gradually decreased by increasing $\Delta\mu$ from 0 to 1 by step size 0.1. Shape relaxation of over 10^7 MCSs was performed under each condition.

IV. RESULTS

For both models, we evaluated the distribution function of the included particles, which is described in Sec. IV A. For the TLP model, both the effective bending coefficient and the surface tension of the vesicle were estimated, and these results

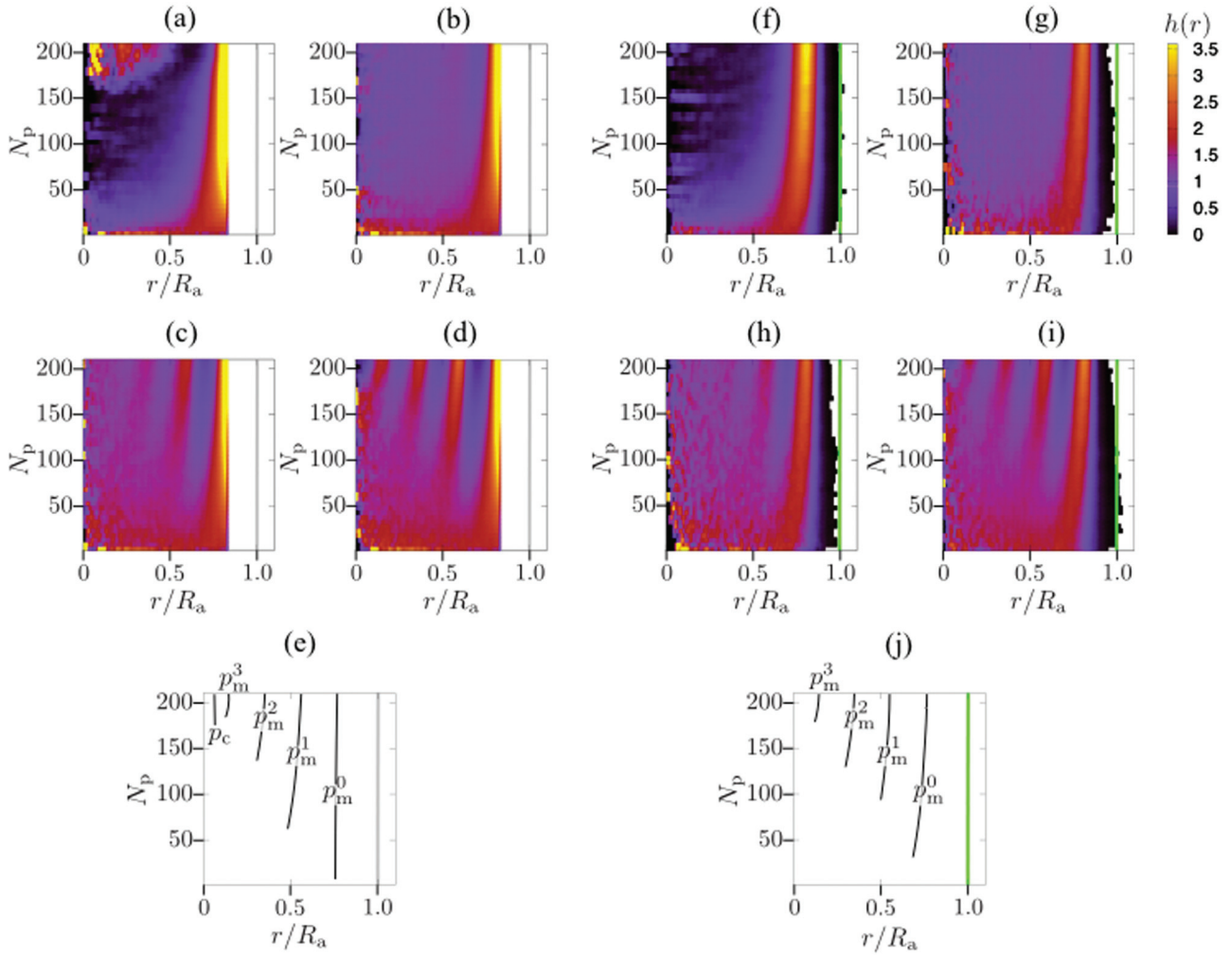

FIG. 5. Distribution function $h(r)$ of the particles in the spherical rigid shell for (a) $n = 1$, (b) $n = 3$, (c) $n = 6$, and (d) $n = 12$ and that of the triangulated lattice for (f) $n = 1$, (g) $n = 3$, (h) $n = 6$, and (i) $n = 12$. The label of each peak is depicted in (e) and (j) for (a)–(d) and (f)–(i), respectively.

are described in Sec. IV B. Finally, we investigated the shape transformation when $\Delta\mu$ is positive in the TLP model, and the summarized results are described in Sec. IV C.

A. Distribution of particles

Snapshots of the equilibrium state of the system with the rigid spherical shell and $N_p = 200$ particles are shown in Fig. 3. For $n = 1$, the particles are localized both near the shell and around the center. For $n = 3$, 6, and 12, the localization is dissolved and particles can be found in the entire interior of the shell.

Snapshots of the equilibrium state of the system with the triangular lattice vesicle and $N_p = 200$ particles are shown in Fig. 4. For $n = 1$, most of the particles are localized near the membrane. For $n = 3$, 6, and 12, the particles are almost randomly distributed inside the vesicles. When $n = 1$, some particles come very close to each other near the membrane.

In order to analyze the particle distribution quantitatively, it is advantageous to consider it along the radial direction. Therefore, the distribution function

$$h(r) = \left\langle \frac{\Delta c(r)}{\Delta V(r)\rho} \right\rangle_{s,t} \tag{19}$$

was defined as a function of the distance r from the center of the shell or the vesicle. Here, $c(r)$ is the number of particles in the interval of the radius between $r - \delta$ and $r + \delta$ with $\delta = 0.25$. In addition, $\Delta V(r)$ is the volume of this interval, and ρ is the particle number density inside the vesicle. The operator $\langle \cdots \rangle_{s,t}$ means averaging over the samples obtained with the different random number seeds and MCSs in the equilibrium state. An error of $h(r)$ is likely to occur at positions extremely close to $r = 0$, as the sampling space there is very small.

The distribution function $h(r)$ of the RSSP model is shown in Figs. 5(a)–5(d). Here, r is scaled by R_a, which is defined by $A_0 = 4\pi R_a^2$. In the distributions for $N_p \leqslant 210$, the maximum number of peaks is two, one, two, and four for $n = 1$, 3, 6, and 12, respectively. The peak observed in the vicinity of the shell [blue line in Fig. 5(e)] is referred to as p_m^0. Then, for $n = 6$ and 12, the peaks occurring in order from the shell side are sequentially referred to as p_m^1, p_m^2, and p_m^3 in

TABLE I. Radial position r/R_a of the peaks of the distribution $h(r)$ of the RSSP model for $N_p = 200$. Peak labels are explained in the caption to Fig. 5(e).

n	p_m^0	p_m^1	p_m^2	p_m^3	p_c
1	0.82				0.09
3	0.82				
6	0.82	0.59	0.36		
12	0.82	0.59	0.38	0.15	

Fig. 5(e). For $n = 1$, the peak near the center of the shell is p_c in Fig. 5(e). The radial position r for $N_p = 200$ is listed in Table I. The smallest observable number of particles of each peak is reported in Table II. The peak series p_m^i ($i = 0, 1, 2, 3$) for $n = 6$ and 12 exhibit an equi-interval, with the distance between neighboring peaks being almost equal to the diameter of the particle when N_p is 200.

The distribution function $h(r)$ of the TLP model is shown in Figs. 5(f)–5(i). The distributions for $n = 1$, 3, 6, and 12 have one, one, two, and four peaks, respectively. The radial position r for $N_p = 200$ and the smallest observable number of particles in each peak are listed in Tables III and IV. These peaks also exhibit an equi-interval for $n = 6$ and 12, with the distance between adjacent peaks being almost equal to the diameter of the particle when N_p is 200.

The height of peak p_m^0 in the TLP model is lower than that of the RSSP model (Fig. 5). Furthermore, the variance of peak p_m^0 in the TLP model is larger than that of the RSSP model. In the TLP model, peak p_c is not observed.

B. Stiffness of the membrane

The effective bending coefficient $\kappa_{\rm eff}$ and effective surface tension $\gamma_{\rm eff}$ of the vesicles under each condition (n, N_p) were evaluated from the fluctuations of the membrane by means of the method in Refs. [30] and [31].

The surface shape of the vesicle $r(\theta, \phi)$ can be expanded [30,31] into spherical harmonics $Y_l^m(\theta, \phi)$ and coefficients $u_l^m(\theta, \phi)$, as

$$r(\theta, \phi) = a\left[1 + \sum_{l=2}^{l_M} \sum_{m=-l}^{l} u_l^m(\theta, \phi) Y_l^m(\theta, \phi)\right]. \tag{20}$$

The cutoff wave number l_M is determined by $(l_M + 1)^2 = N$.

If we consider only the bending energy E_B and surface tension γ, the total energy is $E = E_B + \gamma A$. The excess energy ΔE compared to the energy of the sphere with radius a, which is the average radius of the vesicle, is given by

$$\Delta E = \frac{\kappa_{\rm eff}}{2} \sum_{l=2}^{l_M} \sum_{m=-l}^{l} |u_l^m|^2 (l+2)(l-1)[l(l+1) + Q], \tag{21}$$

where $Q = \gamma_{\rm eff} a^2/\kappa_{\rm eff}$ [31]. If we assume that the averaged excess energy is $\frac{1}{2}k_BT$ for each (l, m),

$$\frac{\langle |u_l^m|^2 \rangle}{a^2} = \frac{k_BT}{\kappa_{\rm eff}} \frac{1}{(l+2)(l-1)[l(l+1) + Q]} \tag{22}$$

is found. To estimate $\kappa_{\rm eff}$ and $\gamma_{\rm eff}$, we employed $\langle |u_l^m|^2 \rangle$ at $l = 2, 3, \ldots, 24$ for $N = 642$ vesicles.

The effective bending coefficient $\kappa_{\rm eff}$ is plotted in Fig. 6(a) as a function of the number of particles N_p for various n's. When N_p is greater than approximately 100, the slope of $\kappa_{\rm eff}/N_p$ for $n = 1$ is much larger than that in the other cases of exponents $n = 3$, 6, and 12. The slopes obtained from the low- and high-N_p regions are listed in Table V.

The effective surface tension $\gamma_{\rm eff}$ is plotted in Fig. 6(b) as a function of the number of particles N_p. When N_p is less than approximately 100, $\gamma_{\rm eff}$ increases similarly for any n, whereas when N_p is greater than approximately 100, the slope becomes steeper for larger n, as reported in Table VI.

C. Transformation of the vesicle

Under the osmotic pressure condition of $\Delta\mu \geqslant 0$ for the TLP model, various shapes of the vesicle appeared in the simulations. The phase diagram of the shapes is described later.

Most of the obtained shapes seem to be almost axisymmetric. In this paper, shapes which fluctuate around the sphere are referred to as "spheres." The shapes of ellipsoids $(x^2/a^2 + y^2/b^2 + z^2/c^2 = 1)$ with $a > b = c$ and $a < b = c$ are referred to as "prolates" and "oblates," respectively. The "stomatocyte" is a shape with a dent. The "discocyte" is a shape with two dents facing each other. The "dumbbell" is a shape which is narrower in the middle than on each end.

TABLE II. The smallest number N_p of particles for which each peak (p_m^i, p_c) appears in the RSSP model [Fig. 5(e)].

n	p_m^0	p_m^1	p_m^2	p_m^3	p_c
1	5				160
3	10				
6	10	60	170		
12	10	55	130	180	

TABLE III. Radial position r/R_a of the peaks of the distribution $h(r)$ of the TLP model for $N_p = 200$ [Fig. 5(j)].

n	p_m^0	p_m^1	p_m^2	p_m^3
1	0.81			
3	0.81			
6	0.81	0.56		
12	0.81	0.58	0.35	0.14

TABLE IV. The smallest number N_p of particles for which each peak (p_m^i) appears in the TLP model [Fig. 5(j)].

n	p_m^0	p_m^1	p_m^2	p_m^3
1	5			
3	5			
6	20	120		
12	20	90	125	175

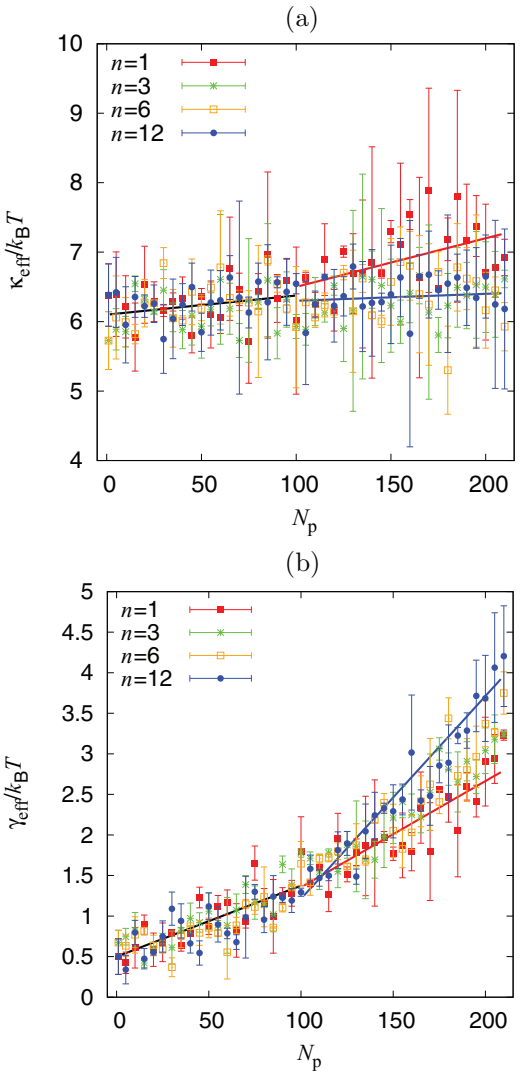

FIG. 6. (a) The effective bending coefficient $\kappa_{\rm eff}$ and (b) the effective surface tension $\gamma_{\rm eff}$ as a function of the number of particles $N_{\rm p}$, for $\kappa = \bar{\kappa} = 10$ and repulsion exponent $n = 1$ (red symbols), $n = 3$ (green symbols), $n = 6$ (orange symbols), and $n = 12$ (blue symbols). Solid lines show the average lines of the best fit for each n with $N_{\rm p}$ in the interval [1:100] (black line), for $n = 1$ with $N_{\rm p}$ in the interval [100:210] (red line), and for $n = 12$ with $N_{\rm p}$ in the interval [100:210] (blue line).

The remaining shapes did not exhibit axial symmetry. During the simulations, the ellipsoid with $a \neq b \neq c$ ("ellipsoid") and the strained discocyte and dumbbell shapes were acquired. In addition, a collapsed shape was obtained, with flat membrane areas and a very large mean curvature edge. The shapes obtained under each condition (n, $N_{\rm p}$) are shown in Fig. 7. To depict the results, which are dependent on the seed of the random numbers, we used a pentagonal symbol including five triangles, where the color of each part corresponds to a certain shape.

For $\Delta\mu = 0$, a sphere was obtained (Fig. 7; blue). The region of the sphere becomes wider with an increasing number of particles $N_{\rm p}$ and the exponent of repulsion of the particles n. When $\Delta\mu$ increases, the shapes deform toward an ellipsoid from a spherical form (Fig. 7; green). The region for $n = 1$ is thinner than the region for $n = 3$, 6, and 12. The shapes transform to a discocyte from the ellipsoid when $\Delta\mu$ increases further (Fig. 7; turquoise). For $N_{\rm p} = 200$, this region was not observed in our simulations. For even larger values of $\Delta\mu$, a stomatocyte is observed when $N_{\rm p} = 50$ (Fig. 7; magenta). For $n = 1$ and $N_{\rm p} = 200$, the region of the dumbbell (Fig. 7; red) is achieved adjacent to the ellipsoid region. The collapsed shape was observed under the conditions $N_{\rm p} = 50$ and $n = 1$ and 3 in the region $\Delta\mu$ (Fig. 7; black). In addition, prolate and oblate shapes were rarely seen, and strained shapes were achieved at the boundary of two axisymmetric shape regions.

TABLE V. Parameters and standard errors obtained for the regression line $\kappa_{\rm eff} = \beta_1 N_{\rm p} + \beta_0$ in the $N_{\rm p}$ intervals [1:100] and [100:210].

	[1:100]		[100:210]	
n	β_1	β_0	β_1	β_0
1	0.002 ± 0.002	6.2 ± 0.1	0.007 ± 0.03	5.8 ± 0.4
3	0.002 ± 0.002	6.1 ± 0.1	0.003 ± 0.02	5.8 ± 0.3
6	0.004 ± 0.002	6.1 ± 0.1	0.001 ± 0.02	6.1 ± 0.4
12	0.003 ± 0.002	6.1 ± 0.1	0.001 ± 0.02	6.2 ± 0.3

V. DISCUSSION

To investigate the relationship between the stiffness of the membrane and the repulsion of the encapsulated particles, we propose two vesicle models. One takes a rigid spherical shell as the vesicle (RSSP model), while the other uses a flexible triangulated lattice as the vesicle (TLP model). Snapshots (Fig. 3 and 4) suggested that particles form layers inside both vesicles. To further investigate these layers, we analyzed the distribution function $h(r)$.

Though repulsive particles tend to separate from each other, they are confined within the vesicles due to the effect of the hard-core repulsion of the wall. For $2 \leqslant N_{\rm p} \lesssim 50$, most particles are arranged in the vicinity of the membrane, $r/R_{\rm a} \gtrsim 0.76$, by the repulsive nature and confinement by the vesicles. In such a state, when a particle is added to the center of the vesicle, the repulsion from the particles near the membrane acts strongly on the added particle. Then the particle moves to the vicinity of the wall, $r/R_{\rm a} \gtrsim 0.76$, so as to minimize the energy of the system. This optimized configuration corresponds to the peak $p_{\rm m}^0$ of $h(r)$ in Fig. 5. Especially for $n = 1$, the result corresponds to the

TABLE VI. Parameters and standard errors obtained for the regression line $\gamma_{\rm eff} = \beta_1 N_{\rm p} + \beta_0$ in the $N_{\rm p}$ intervals [1:100] and [100:210].

	[1:100]		[100:210]	
n	β_1	β_0	β_1	β_0
1	0.010 ± 0.002	0.48 ± 0.09	0.013 ± 0.002	0.1 ± 0.3
3	0.010 ± 0.001	0.51 ± 0.08	0.016 ± 0.001	-0.1 ± 0.2
6	0.007 ± 0.001	0.51 ± 0.08	0.018 ± 0.002	-0.5 ± 0.3
12	0.008 ± 0.001	0.50 ± 0.08	0.025 ± 0.002	-1.3 ± 0.2

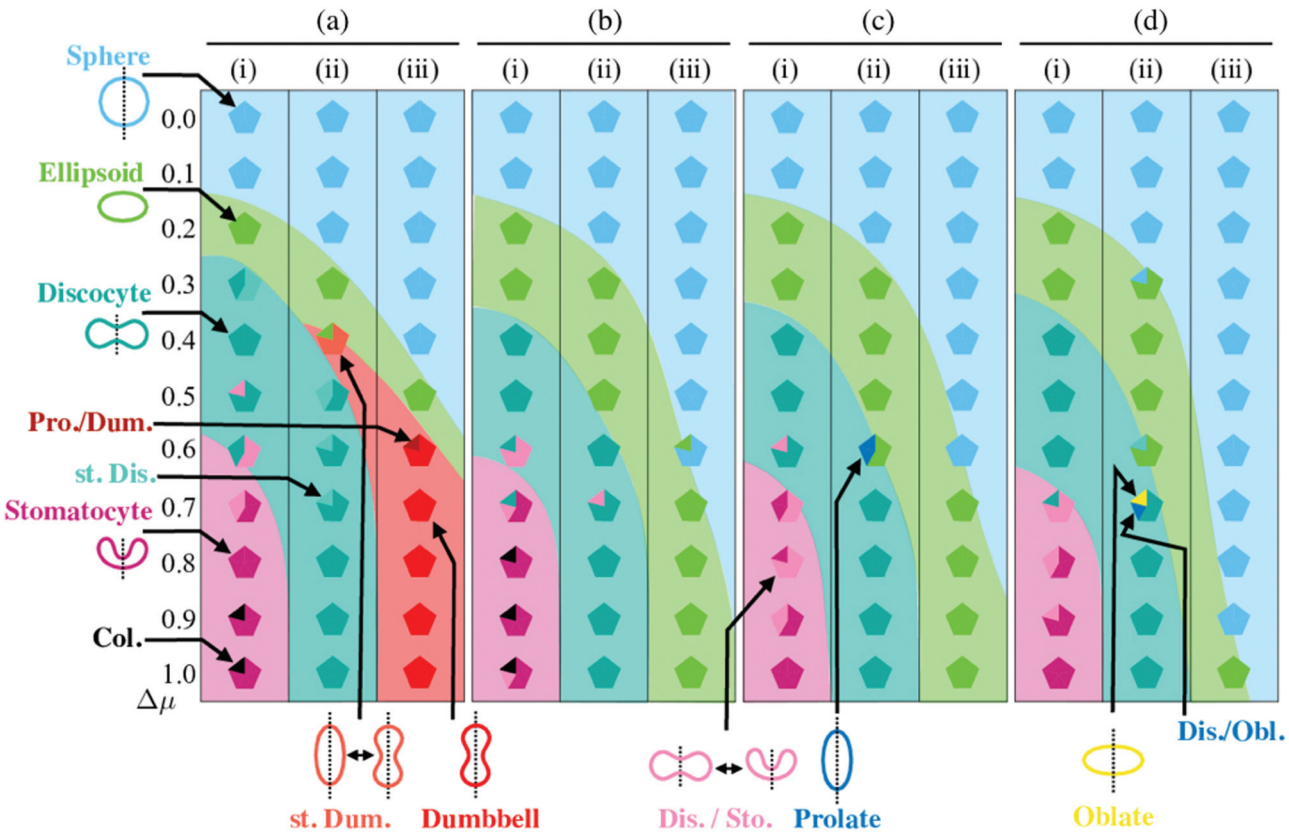

FIG. 7. Simulation results of the shape transformation that reduces the volume. The pentagonal symbol has five triangles, with the color of each triangle corresponding to the shape. (a) $n = 1$, (b) $n = 3$, (c) $n = 6$, and (d) $n = 12$. The number aligned vertically is $\Delta\mu$. (i), (ii), and (iii) indicate $N_p = 50$, 100, and 200, respectively. The sphere is blue. The ellipsoid is green. The strained discocyte (st. dis.) is mint. The discocyte is turquoise. The repetitions of discocyte and stomatocyte (dis./sto.) are pink. The stomatocyte is magenta. The strained dumbbell is light orange. The repetitions of prolate and dumbbell (pro./dum.) are brown. The dumbbell is red. The prolate is dark blue. The oblate is gray. The repetitions of discocyte and oblate (dis./obl.) are orange. The collapsed shape (col.) is black.

electrostatic phenomenon in which charges are distributed on the surface of conductors. When the number of particles exceeds a certain number, some particles are arranged in the center of the vesicle, away from the membrane, so as to minimize the energy of the system. As a result, peaks p_c and p_m^1 of $h(r)$ have appeared in Fig. 5. Therefore, the difference in repulsive energy between the radial direction and the angular direction dominates the stable configuration of particles. In the case of particles with short-range repulsion, the particles can be located in the middle region, $0.12 \lesssim r/R_a \lesssim 0.76$, because the repulsive energy between distant particles is low. The particles gathered into the layer form as a new wall, whereupon multiple layers are recursively formed inside the vesicle. Particles with long-range repulsion are rarely seen in the middle region. In contrast, particles with short-range repulsion are often arranged in the middle region. In the TLP model, the arrangement of the particles around p_m^0 changes according to the vesicular shape, and the whole energy of the vesicle also changes. As a result, the arrangement of the particles on the center side becomes unstable, as shown in the absence of peak p_c in Fig. 5(f). In addition, because the radius of the RSSP model and the average radius of the TLP model are equal, the storage area of particles near the membrane surface is larger in the TLP model. Therefore, the formation of the particle layer near the center of the vesicle is suppressed. For these reasons, peak p_c is not observed in the TLP model. The number of peaks of $h(r)$ which appeared in the TLP model is smaller than that in the RSSP model (Tables I and III). Under the constraint of the wedge, an arrangement of particles is formed from the narrow corner [41]. This result agrees with our result, which shows that the order of particles begins in a narrow domain.

In order to investigate the effect of the internal particles on the stiffness of the membrane, we estimated the effective bending coefficient $\kappa_{\rm eff}$ and the effective surface tension $\gamma_{\rm eff}$ from the fluctuation of the vesicular membrane. From these results, we found that $\kappa_{\rm eff}$ is always smaller than κ. If we use the equation $\kappa_{\rm eff}^r = \kappa - [3k_BT/(4\pi)]\ln(l_M)$, where only the excess bending energy is assumed to contribute to the total excess energy [53–56], $\kappa_{\rm eff}^r$ is about 0.9κ, which is larger than our results. However, we separated the excess energy from the bending energy and the surface tension in our analysis, therefore the pure $\kappa_{\rm eff}$ is obtained, which is smaller than $\kappa_{\rm eff}^r$. We also found that the effective surface tension $\gamma_{\rm eff}$ as a function of N_p for $n = 12$ rapidly increased at $N_p = 100$, where the packing fraction of the particles $(4/3)\pi(\sigma_p/2)^3/V$ is 0.25. This is consistent with the characteristic of surface tension obtained in a numerical study using hard spheres and a hard wall [39]. The major part of the excess energy of the vesicle is due to surface tension γA. The effective

bending coefficient is almost independent of N_p with an exception in the case of $n = 1$. This is because the pressure and surface tension are increased as represented by the Young-Laplace equation. This equation is a linear function of $\Delta\mu$ when the curvature is fixed. However, the effective internal pressure should be described as a nonlinear function of N_p. As a result, the effective surface tension is a nonlinear function of N_p. When $n = 1$, the equation is considered to be invalid since the internal pressure is anisotropic.

For $N_p \lesssim 100$, the value of neither $\kappa_{\rm eff}$ nor $\gamma_{\rm eff}$ is dependent on the exponent n. Therefore, it is suggested that the deformation of the vesicle due to the change in osmotic pressure is independent of n when N_p is small. For $N_p \gtrsim 100$ in Fig. 6, deformation depends on n. Comparing the case of $n = 1$ with the other cases, it is suggested that the particles with long-range repulsion ($n = 1$) strongly suppress the fluctuation of the mean curvature H_i of the vesicular membrane. On the other hand, the particles suppress the fluctuation of the surface area A weakly. This suggests that the short-range repulsion of particles suppresses the large deformation of the vesicular shape that is observed when $n = 1$ (Fig. 7).

The shapes of the vesicles with a reduced volume were simulated by increasing the osmotic pressure difference $\Delta\mu$. As shown in the phase diagram ($\Delta\mu$, N_p) in Fig. 7, only under the condition $n = 1$ and $N_p = 200$ were dumbbell-shaped vesicles obtained. This shape is reminiscent of the twin shape observed experimentally [2,4]. For the same Δa_0 value, the shape of the vesicle without included particles becomes a discocyte with a lower energy, rather than a dumbbell [16]. Therefore, even if the vesicle contains particles, if $n = 3$, 6, or 12, their repulsion is not strong enough to overcome the stiffness of the membrane and the shape of the vesicles settles as a discocyte. However, in the case of $n = 1$, when the number of particles in the vesicle increases, the number density of the particles in the particle layer (p_m^0) in the vicinity of the membrane becomes nonuniform, so that two regions with relatively high number densities (two polar regions) are generated on two opposite sides. By long-range repulsion acting between the two polar regions, the vesicle is extended along the axis passing through both poles while maintaining the size of the polar regions [Fig. 8(a)]. As a result, at $\Delta\mu > 0$, the equatorial portion of the vesicle becomes narrow, reducing the volume of the vesicle. In such a process, dumbbell shapes have been induced as a result of particle-vesicle interaction. For a negative osmotic pressure, $\Delta\mu < 0$, experiments and theoretical studies in Refs. [48], [57], and [58] were conducted to polymerize microtubules encapsulated in a vesicle, and deformation of a vesicle into a lollipop shape was observed by the MMC simulation [Fig. 8(b)]. Polymerized microtubules stretch in one direction, as shown in Fig. 8(b). The end regions [circles in Fig. 8(b)], which are in contact with the membrane, can be considered the polar regions repelled through the long-range repulsion in our model, as shown in Fig. 8(a). According to this analogy, even in a vesicle containing particles with a negative $\Delta\mu$, there exists the possibility that protrusions, as seen in the lollipop shape, will occur. The sign of the osmotic pressure difference $\Delta\mu$ determines which shape will be assumed, dumbbell or lollipop.

In order to analyze the stiffness of the membrane, we employed Eq. (22). If the term Q in Eq. (22) is neglected and the change in the small area is considered, the fitting error of the stiffness estimation is reduced. However, the stiffnesses of the bending and stretching are essentially different and need to be analyzed separately. By separating these two changes, it is possible to investigate the effect of the particles.

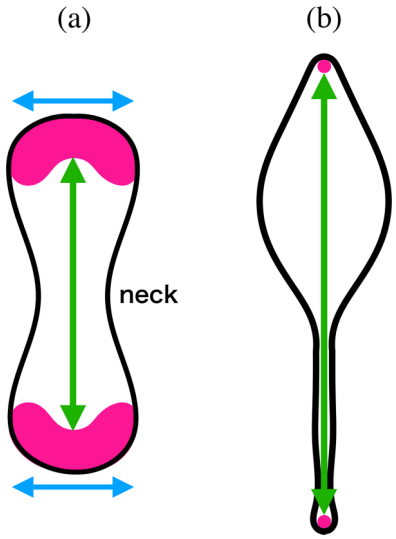

FIG. 8. Illustrations of (a) the dumbbell shape with particle clusters (corresponding to $n = 1$, $N_p = 200$, $\Delta\mu = 0.6$) and (b) the lollipop shape with two particles [48]. Arrows show the repulsion between particles. The repulsion between separated particles is shown in green, and the repulsion between neighboring particles is shown in blue.

The exponent n is a characteristic feature related to the range of the repulsion between two particles. However, it is difficult to extract the exponent from the interaction of complex colloidal particles because it is necessary to examine not only the entropy but also the internal energy. For example, the intramolecular interaction in a colloidal particle made of a polymer, which is often referred to as the excluded-volume effect among those monomers, is regarded to have a long-range nature [59]. Therefore, the strength of the interaction between these two colloids is related to the monomer density in each colloid. We expect that the larger spatial variance of the distribution $g(r)$, where r is the distance of a monomer from the center of the polymer chain, corresponds to the longer range of the repulsive force between these colloids. The variance should be a function of the degree of polymerization, microscopic length, or magnitude of intramolecular repulsion of the monomers. Consequently, it is considered that the steric interaction among the deformable colloidal particles, which we call "soft repulsion" in this work, is an important factor determining the range of the interaction between these colloids.

In our model, we take into account the soft-core repulsion of encapsulated particles, so that the transformations of the vesicles mainly occurred by minimizing the internal energy. Our results do not exclude the possibility that depletion interaction induces transformation of the vesicle. However, we confirmed that the long-range steric repulsive interaction between particles induces transformation. If we consider the steric interaction shielded by the membrane and the particles

within it, the neck of the dumbbell may become narrower and may show two spheres.

Although simple long-range repulsion, such as the Coulomb force acting between particles, is not effective in the solution, the collective effect of the internal structure, such as the microtubule extending into the vesicle [Fig. 8(b)], and the coherent structures of particles may generate long-range interactions that act between regions of the membrane.

VI. CONCLUSION

We performed Monte Carlo simulations with the RSSP and TLP models of a vesicle containing numerous soft-core particles. The results of both models were analyzed by means of the distribution of the int ernal particles. In addition, in order to evaluate the effect of particles on the vesicular shape and the stiffness of the membrane, we used the TLP model.

With an increase in the number of internal particles, the effective bending coefficient and surface tension increased. In comparison, the long-range repulsive particles resulted in a greater bending elastic coefficient. Furthermore, the short-range repulsive particles induced a greater surface tension. This fact suggests that long-range repulsion promotes large deformations of the vesicle. When the volume of the vesicle containing particles decreased, the particles with long-range repulsion caused a dumbbell shape, which is similar to the twin vesicle observed experimentally [2,4]. We found that the repulsion between the flexible vesicle and the particle layers (p^i_{m}) contributes to the transformation of the vesicular shape into the dumbbell shape. Analysis of the particle distribution showed that the particles were stratified depending on the exponent of the repulsion. It is unknown yet whether this stratification is experimentally observable. If the experimental observation technique is enhanced, a comparison of our results and the experimental results will be possible. To reproduce the large deformation together with the distribution of particles, it is necessary to consider other effects, such as a locally different osmotic pressure and an enhancement of the lipid exchange rate depending on the membrane curvature.

We showed that the behavior and structure of collective particles are important for understanding the shape of vesicles including particles. In order to evaluate these effects, a study with a large number of particles will be necessary.

Further studies with various sizes of the particles and membrane and also with various strengths of repulsion between particles should be performed, and the model under consideration of shielding of repulsion is needed as a more realistic model.

We believe that our results will help further studies. Perhaps organisms may utilize different repulsive forces depending on the molecules participating in the involved biological events.

[1] S. B. Zimmerman and A. P. Minton, Annu. Rev. Biophys. Biomol. Struct. **22**, 27 (1993).
[2] Y. Natsume, O. Pravaz, H. Yoshida, and M. Imai, Soft Matter **6**, 5359 (2010).
[3] Y. Natsume and T. Toyota, PLoS One **11**, e0146683 (2016).
[4] H. Terasawa, K. Nishimura, H. Suzuki, T. Matsuura, and T. Yomo, Proc. Natl. Acad. Sci. USA **109**, 5942 (2012).
[5] S. Asakura and F. Oosawa, J. Chem. Phys. **22**, 1255 (1954).
[6] S. Asakura and F. Oosawa, J. Polym. Sci. **33**, 183 (1958).
[7] Y. Mao, M. E. Cates, and H. N. W. Lekkerkerker, Physica A **222**, 10 (1995).
[8] A. D. Dinsmore, D. T. Wong, P. Nelson, and A. G. Yodh, Phys. Rev. Lett. **80**, 409 (1998).
[9] W. Li and H. R. Ma, Phys. Rev. E **66**, 061407 (2002).
[10] L. Rovigatti, N. Gnan, A. Parola, and E. Zaccarelli, Soft Matter **11**, 692 (2015).
[11] H. Noguchi, J. Phys. Soc. Jpn. **78**, 041007 (2009).
[12] J. E. Rothman and E. A. Dawidowcz, Biochemistry **14**, 2809 (1975).
[13] P. B. Canham, J. Theor. Biol. **26**, 61 (1970).
[14] W. Helfrich, Z. Naturforsch. C **28**, 693 (1973).
[15] J. N. Israelachvili, D. J. Mitchell, and B. W. Ninham, Biochim. Biophys. Acta **470**, 185 (1977).
[16] U. Seifert, K. Berndl, and R. Lipowsky, Phys. Rev. A **44**, 1182 (1991).
[17] L. Miao, U. Seifert, M. Wortis, and H.-G. Döbereiner, Phys. Rev. E **49**, 5389 (1994).
[18] S. Svetina and B. Žekš, Eur. Biophys. J. **17**, 101 (1989).
[19] K. Khairy and J. Howard, Soft Matter **7**, 2138 (2011).
[20] A. Sakashita, N. Urakami, P. Ziherl, and M. Imai, Soft Matter **8**, 8569 (2012).
[21] H. W. Gerald Lim, M. Wortis, and R. Mukhopadhyay, Proc. Natl. Acad. Sci. USA **99**, 16766 (2002).
[22] Y. Kantor, M. Kardar, and D. R. Nelson, Phys. Rev. A **35**, 3056 (1987).
[23] S. Svetina, ChemPhysChem **10**, 2769 (2009).
[24] D. M. Kroll and G. Gompper, Science **255**, 968 (1992).
[25] D. H. Boal and M. Rao, Phys. Rev. A **45**, R6947 (1992).
[26] G. Gompper and D. M. Kroll, Phys. Rev. E **52**, 4198 (1995).
[27] P. B. S. Kumar, G. Gompper, and R. Lipowsky, Phys. Rev. Lett. **86**, 3911 (2001).
[28] G. Gompper and D. M. Kroll, J. Phys. I France **6**, 1305 (1996).
[29] C. Itzykson, in *XVI GIFT International Seminar on Theoretical Physics*, edited by J. Abad, M. Asorey, and A. Cruz (World Scientific, Singapore, 1986), pp. 130–188.
[30] M. B. Schneider, J. T. Jenkins, and W. W. Webb, J. Phys. **45**, 1457 (1984).
[31] S. T. Milner and S. A. Safran, Phys. Rev. A **36**, 4371 (1987).
[32] G. Gompper and D. M. Kroll, Europhys. Lett. **19**, 581 (1992).
[33] G. T. Linke, R. Lipowsky, and T. Gruhn, Phys. Rev. E **71**, 051602 (2005).
[34] E. Haleva and H. Diamant, Phys. Rev. Lett. **101**, 078104 (2008).
[35] G. Gompper and D. M. Kroll, Phys. Rev. E **51**, 514 (1995).
[36] F. F. Abraham W. E. Rudge, and M. Plischke, Phys. Rev. Lett. **62**, 1757 (1989).

[37] D. R. Nelson and L. Peliti, J. Phys. **48**, 1085 (1987).
[38] E. Trizac and J.-L. Raimbault, Phys. Rev. E **60**, 6530 (1999).
[39] M. Heni and H. Löwen, Phys. Rev. E **60**, 7057 (1999).
[40] A. Fortini and M. Dijkstra, J. Phys.: Condens. Matter **18**, L371 (2006).
[41] B. V. R. Tata, D. Boda, D. Henderson, A. Nikolov, and D. T. Wasan, Phys. Rev. E **62**, 3875 (2000).
[42] M. Fošnarič, A. Iglič, D. M. Kroll, and S. May, J. Chem. Phys. **131**, 105103 (2009).
[43] A. Šarić and A. Cacciuto, Phys. Rev. Lett. **109**, 188101 (2012).
[44] H. Itoga, R. Morikawa, T. Miyakawa, H. Yamada, Y. Natsume, T. Ueta, and M. Takasu, JPS Conf. Proc. **5**, 011002 (2015).
[45] H. Noguchi and G. Gompper, Proc. Natl. Acad. Sci. USA **102**, 14159 (2005).
[46] X. Li, B. Caswell, and G. E. Karniadaks, Biophys. J. **103**, 1130 (2012).
[47] J.-S. Ho and A. Baumgärtner, Europhys. Lett. **12**, 295 (1990).
[48] R. Morikawa, Y. Saito, and H. Hyuga, J. Phys. Soc. Jpn. **68**, 1760 (1999).
[49] A. Guckenberger and S. Gekle, J. Phys.: Condens. Matter **29**, 203001 (2017).
[50] E. A. Evans, Biophys. J. **14**, 923 (1974).
[51] A. Einstein, Ann. Phys. **322**, 549 (1998).
[52] M. Matsumoto and T. Nishimura, TOMACS **8**, 3 (1998).
[53] D. R. Nelson, T. Piran, and S. Weinberg (eds.), *Statistical Mechanics of Membranes and Surfaces*, 2nd ed. (World Scientific, Singapore, 2004).
[54] W. Cai, T. C. Lubensky, P. Nelson, and T. Powers, J. Phys. II (France) **4**, 931 (1994).
[55] W. Helfrich, J. Phys. (France) **46**, 1263 (1985).
[56] L. Peliti and S. Leibler, Phys. Rev. Lett. **54**, 1690 (1985).
[57] H. Hotani and H. Miyamoto, Adv. Biophys. **26**, 135 (1990).
[58] T. Umeda, H. Nakajima, and H. Hotani, J. Phys. Soc. Jpn. **67**, 682 (1998).
[59] H. Yamakawa, *Modern Theory of Polymer Solutions* (Harper & Row, New York, 1971).